

Direct evidence of nodeless clean superconductivity and determination of the superfluid density in single-layer FeSe grown on SrTiO₃

P. K. Biswas,^{1,*} Z. Salman,¹ Q. Song,² R. Peng,² J. Zhang,² L. Shu,² D. L. Feng,² T. Prokscha,¹ A. Suter,¹ and E. Morenzoni^{1,†}

¹Laboratory for Muon Spin Spectroscopy, Paul Scherrer Institut, CH-5232 Villigen PSI, Switzerland

²State Key Laboratory of Surface Physics, Department of Physics, Fudan University, Shanghai 200433, China

(Dated: February 9, 2016)

Bulk FeSe is superconducting with a critical temperature $T_c \cong 8$ K and SrTiO₃ is insulating in nature, yet a T_c as high as 109 K has been reported at the interface between a single-layer FeSe and SrTiO₃. Angle resolved photoemission spectroscopy and scanning tunneling microscopy measurements observe a gap opening at the Fermi surface below ≈ 60 K. Elucidating the microscopic properties and understanding the pairing mechanism of single-layer FeSe is of utmost importance as it is the basic building block of iron-based superconductors. Determining microscopic length scales such as the magnetic penetration depth, detecting the homogeneity of the superconducting state and the possible presence of magnetism remain key issues. Here, we use the low-energy muon spin rotation/relaxation technique (LE- μ SR) to detect and quantify the superfluid density and determine the gap symmetry in a single-layer of FeSe grown on SrTiO₃ (100). Measurements in applied field show a temperature dependent broadening of the field distribution below ~ 60 K. Zero field measurements rule out the presence of magnetism of static or fluctuating origin. From the inhomogeneous field distribution, we determine an effective penetration depth of $\lambda \cong 112$ nm at $T \rightarrow 0$ K, which corresponds to all carriers in the single layer being paired. The temperature dependence of the superfluid density $n_s(T)$ can be well described by simple s -wave BCS, indicating a clean nodeless superconducting state with a gap of 10.2(1.1) meV. The result is a clear indication of the gradual formation of a two dimensional vortex lattice existing over the entire large FeSe/STO interface and provides unambiguous evidence for robust clean superconductivity in buried single-layer FeSe.

Following the discovery of high- T_c cuprates [1, 2] a few decades ago, the recently discovered Fe-based superconductors [3–8] represent a novel and important class of high- T_c superconductors. Surprisingly, high-temperature superconductivity in single-layer FeSe on SrTiO₃ (STO) with a $T_c \approx 60$ K [9–13] exceeds T_c of all known bulk iron-based superconductors. This discovery is extremely important in view of the simple crystal structure of the system, which consists of a single Se-Fe-Se unit, i.e. the basic building block of all iron-chalcogenide superconductors, and may pave the way to identifying key ingredients of high- T_c superconductivity [10, 11]. Single-layer FeSe exhibits a distinct electronic structure with only electron pockets near the Brillouin zone corner [11–13]. This is in contrast to its bulk counterpart, that also shows hole pockets at the zone center. Transport measurements performed *ex situ* on single-layer FeSe, capped by layers of FeTe and amorphous Si, show zero-resistivity below 23.5 K with an onset T_c of 40 K [16]. However, *in situ* zero-resistivity was detected at a temperature as high as 109 K [17]. Diamagnetic shielding was also observed at ~ 65 K and attributed to the Meissner effect [18]. Scanning tunneling microscopy and ARPES measurements suggest that single-layer FeSe has plain s -wave pairing symmetry [10–12, 19]. Very recently, it has been shown that electrochemically etched ultrathin FeSe also exhibits superconductivity around 40 K under application of an electric field, regardless of the substrate material [20]. Nonetheless, all experiments performed to date do

not provide conclusive evidence that the gap appearing below ~ 60 K is only related to the formation of a condensate of Cooper pairs and do not exclude other possibilities such as magnetic, charge or spin density wave gaps. Determination of the superfluid density and of the homogeneity of the superconducting phase remain to be addressed.

Here, we report detailed depth resolved investigation of the superconducting and magnetic properties in single-layer FeSe by the low-energy muon spin rotation/relaxation (LE- μ SR) technique. Zero field (ZF) μ SR measurements clearly demonstrate that the ground state of single-layer FeSe is non-magnetic and transverse field (TF) μ SR results show that superconductivity appears below 62 K. Taking into account the extreme 2D-character of the vortex state, we estimate the effective penetration depth, $\lambda \cong 112$ nm at $T \rightarrow 0$ K. The superfluid density $n_s(T) \approx \lambda^{-2}(T)$ is well described by a simple BCS s -wave model indicating a nodeless superconducting state involving all carriers in the single-layer FeSe.

Single-layer FeSe was grown using molecular beam epitaxy on a 0.5% Nb doped SrTiO₃ (001) and capped by four additional layers of FeSe and a ~ 25 nm protective layer of amorphous Se. The additional layers act as stabilizer and do not superconduct [9, 11, 12]. Details of the sample preparation are described in the Methods section. Figure 1 shows a schematic of the heterostructure used in this experiment. The LE- μ SR experiments were

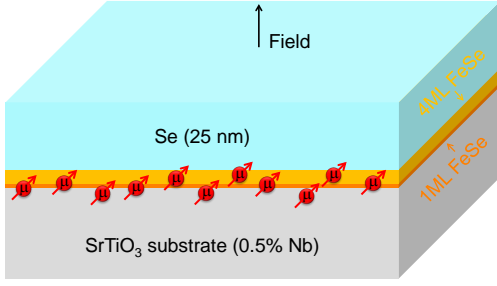


FIG. 1: **Layers of the heterostructure.** Schematic diagram (not to scale) of the heterostructure with a the single-layer FeSe film grown on SrTiO₃ substrate. The polarization of the implanted muons is parallel to the sample surface.

performed on the LEM instrument, at the Paul Scherrer Institut in Villigen, Switzerland [21, 22]. Here it is possible to tune the implantation energy of fully polarized muons, thus varying their stopping depth and allowing to probe the magnetic response in different layers of the heterostructure. Further details about LE- μ SR are described in the Methods section.

Initially, we tune the muon beam implantation energy, E , to maximize the fraction of muons stopping in the vicinity of the FeSe single-layer. Monte Carlo simulations, presented in Figure 2, show that this is achieved using $E \sim 3$ keV. The program TRIM.SP, specially modified for muon implantation in heterostructures, and whose reliability to calculate stopping profiles has been previously tested, was used for the calculation [23, 24].

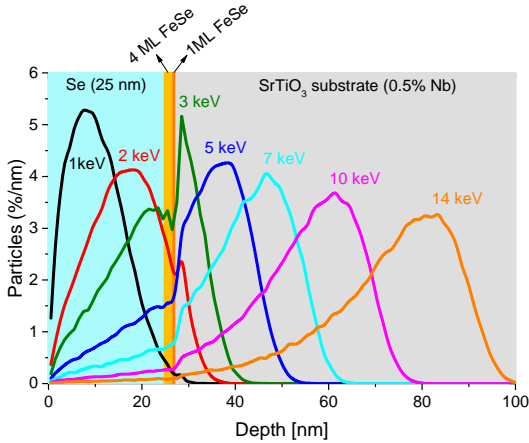


FIG. 2: **Muon implantation profiles.** Muon stopping profiles in the investigated heterostructure calculated at different implantation energies using the Monte Carlo code TRIM.SP.

Using this implantation energy we performed TF- μ SR measurements as a function of temperature. For these

measurements, the sample was cooled in a magnetic field of 10 mT applied normal to the sample surface and to the initial muon spin direction. We find that the muon spin polarization follows a Gaussian damped precession function, as shown in the supplementary information Fig. 7. The temperature dependence of the Gaussian damping rate σ is shown in Fig. 3 and displays a clear increase on lowering the temperature. This is due to the inhomogeneous field distribution associated with the formation of the vortex state in the superconducting single-layer FeSe forming below ~ 60 K. Our value of T_c agrees well

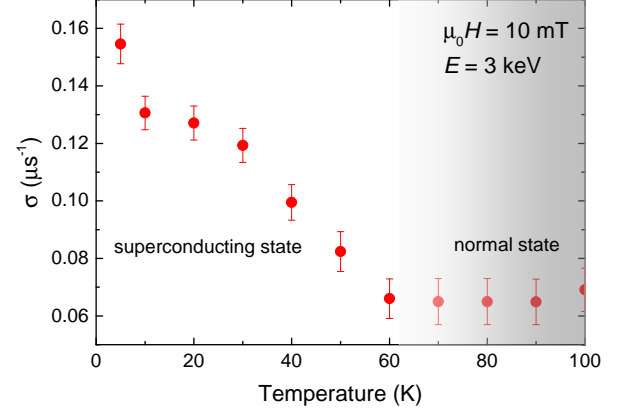


FIG. 3: **Temperature dependence of the muon spin damping rate.** The temperature dependence of the muon spin damping rate σ measured at an implantation energy of 3 keV and an applied field of 10 mT.

with the temperature for gap opening observed in several ARPES measurements [9–13]. In principle broadening could be caused by magnetism. However, in a ZF measurement, which is very sensitive to magnetism, we do not detect any difference in the spectra taken at 5 K and 100 K, as shown in Fig. 4. This observation rules out broadening due to magnetism of static or dynamic origin and confirms a direct observation of the formation of a vortex lattice in superconducting single-layer FeSe with $T_c \sim 60$ K.

The damping of the TF- μ SR signal is proportional to the width of the magnetic field distribution in the vortex state $\sigma = \gamma_\mu \sqrt{\Delta B^2}$ (γ_μ is the muon gyromagnetic ratio). The measurement of the field distribution in the vortex state or its moments by μ SR is a powerful technique to determine the magnetic penetration depth and its temperature dependence $\lambda(T)$ [25]. $\lambda(T)$ is related to the effective superfluid density, $\lambda^{-2}(T) \propto \frac{n_s(T)}{m^*}$, where n_s is the density of superconducting carriers and m^* their effective mass. The low-temperature behavior of the magnetic penetration depth reflects the superconducting gap structure. For a fully gapped s -wave superconductor, where $\Delta\lambda(T) = \lambda(T) - \lambda(0)$ decays exponentially, there

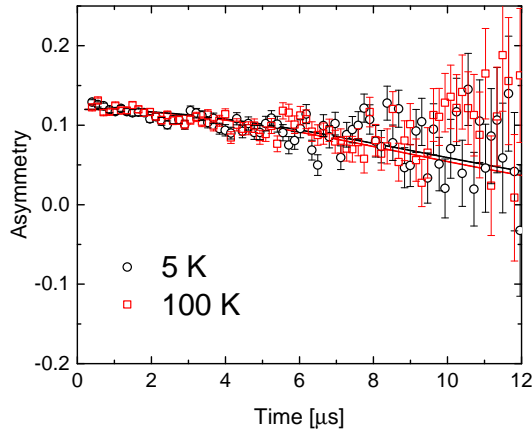


FIG. 4: **ZF muon spin relaxation.** ZF- μ SR time spectra collected at 5 K and 100 K for single-layer FeSe with muon implanted at an energy of 2.3 keV. The solid lines are fits to the data. See supplemental information for details about the fit function.

is no pronounced temperature dependence at low temperature, whereas it increases linearly in a nodal superconductor [25].

The measurement of σ as a function of depth by varying the muon implantation energy, E , further establishes the source of the observed superconductivity, (Figure 5). As expected from the TRIM.SP calculations, we observe

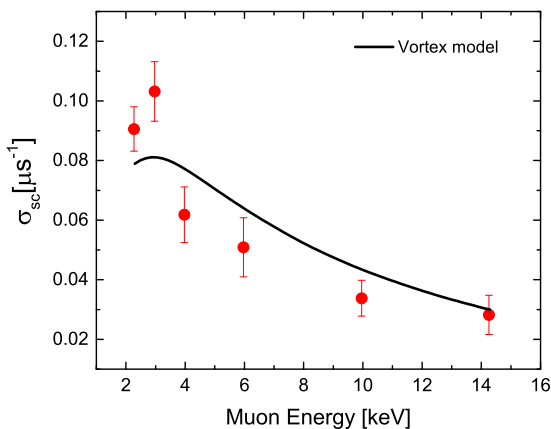


FIG. 5: **Energy dependence of the field broadening.** Muon spin damping rate σ_{sc} after correction of the nuclear moments contribution plotted as a function of muon implantation energy E . The solid line shows the fit where the σ_{sc} vs. E curve has been calculated within a London model of a very thin superconducting layer as described in the text and in the supplement.

the largest field inhomogeneity at ~ 3 keV, where most of the muons are implanted very close to the single-layer FeSe.

The observed broadening can be expressed by $\sigma(T) = (\sigma_{sc}^2(T) + \sigma_{nm}^2)^{\frac{1}{2}}$, where σ_{sc} is the contribution to the field broadening due to the superconducting state in single-layer FeSe, and σ_{nm} is caused by the dipolar field contribution of the nuclear moments. The latter is small and temperature independent but slightly depends on the muon implantation energy due to the different nuclear moment contribution in the various layers composing the heterostructure. We determined this contribution by performing a full energy scan in the normal state at $T = 100$ K. $\sigma_{sc}(T)$ is determined by the 2D pancake vortices that form in a thin superconducting layer [6, 26]. Since the muon stopping profile encompasses a region outside the single FeSe layer (see Fig 2), the inhomogeneous stray field of the vortices, which extends outside the superconducting layer [6, 28], has to be taken into account to obtain the relationship between $\sigma_{sc}(T)$ and the effective magnetic penetration depth in a single-layer FeSe.

The field profile and distribution have been obtained by solving the London equation via Fourier transform with source terms representing the flux line to describe the spatial variation of $B_z(x, y, z)$ in a single FeSe layer of thickness d ($-d/2 < z < d/2$, x, y planar coordinates), whereas outside the superconducting layer B_z obeys Laplace equation. Details of this calculation are given in the supplemental information.

For a bulk superconductor in the vortex state the length scale of the field broadening is directly given by the magnetic penetration depth $\sigma_{sc} \propto \frac{1}{\lambda^2}$. In contrast, in our 2D situation we find that the field broadening is governed by the Pearl length scale $\Lambda_P \equiv 2\lambda^2/d$ as expected for the vortex state in superconducting films with $d \ll \lambda$ [29]. For a comparison with the measured broadening, $\Delta B_z(z)$ has to be weighted with the normalized muon stopping distribution $n(z, E)$ so that $\sigma_{sc}^2(E) = \gamma_\mu^2 \int_{-\infty}^{\infty} \Delta B_z^2(z) n(z, E) dz$. Fitting the measured energy dependence of $\sigma_{sc}(E)$ (Fig. 5) with our model we determine $\Lambda_P = 2.04(5) \times 10^4$ nm at low temperatures. Assuming an effective thickness of the superconducting FeSe single-layer of 1 nm this gives a magnetic penetration depth $\lambda = 112(5)$ nm at $T \rightarrow 0$ K.

From our determination of λ , we estimate the density of paired electrons to be $n_s(0) = \frac{m^*}{\mu_0 e^2 \lambda^2(0)} \simeq 6.08 \times 10^{21}$ cm $^{-3}$ (where we used for the effective mass $m^* = 2.7m_e$ from [12]). ARPES measurements of the electronic structure of single-layer FeSe with $T_c \approx 60$ K give an electron counting of ~ 0.12 electron/Fe [11, 12]. This corresponds to a carrier concentration $n_e \approx 6 \times 10^{21}$ cm $^{-3}$ in very good agreement with our estimate, thus indicating that practically all carriers present in the single-layer condense in the superconducting state and that single-layer FeSe is

a clean superconductor. It should be remarked that inclusion of disorder in the vortex lattice does not change these conclusions. The effect of disorder is to increase the value of λ . However, disorder adds only quadratically to the measured spin relaxation rate so that even a contribution equal to the broadening associated with the vortex field would increase λ just by $\sim 20\%$. Our conclusions are equally unaffected by another choice of d , which we took as an average between the lattice constant of the single layer and the coherence length.

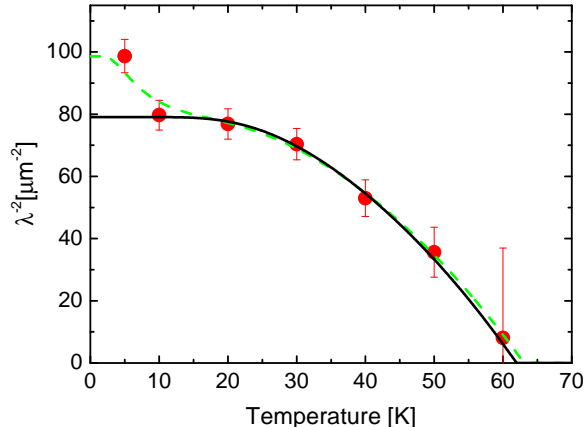


FIG. 6: **Temperature dependence of the superfluid density.** $1/\lambda^2$ versus temperature for single-layer FeSe. The solid curve is a fit with a BCS s -wave gap. For comparison a model assuming an additional small gap manifesting itself at low temperatures is shown as a dashed line.

Figure 6 shows the temperature dependence of $1/\lambda^2$, which is proportional to the superfluid density in single-layer FeSe. Remarkably, $1/\lambda(T)^2$ does not show any signature of quantum phase fluctuations, probably because of the strong coupling to the STO substrate [10] and can be well fitted down to 10 K using a single-gap BCS s -wave model (solid line in Fig. 6). The fit gives a gap value at zero temperature $\Delta(0) = 10.2(1.1)$ meV and $T_c = 62(2)$ K. This gap value is consistent with several ARPES and STM measurements that find values in the range 10-15 meV [10–13, 15]. Some STM measurements have reported gap structures with double peaks at ≈ 10 meV and 15-20 meV [9]. These differences may be due to differences in annealing conditions of the sample, protection layer or substrate preparation. It is worth noting that since the muons probe uniformly the entire area of the sample, the measured parameters are sample average values. μ SR also discriminates between different phases; all our TF- μ SR data can be fitted with a single superconducting component. Therefore, the results show that homogeneous superconductivity exists across the entire FeSe/STO interface of size $\sim \text{cm}^2$. The gap to T_c ratio

$\frac{\Delta(0)}{k_B T_c} = 1.9(2)$ puts the single-layer FeSe in the category of the moderately strong-coupling superconductors.

The temperature dependence of the superfluid density (Fig. 6) may suggest an increase of this quantity at the lowest measured temperature, 5 K. Since this effect appears only in a single data point we can only speculate about its significance. It might point to the presence of a second (small) gap effectively opening below 10 K. We tried a two gap $s+s$ wave model to account for this low temperature increase. A fit is shown as dashed line in Fig. 6 yielding for the main gap $\Delta(0) = 10.5(1.6)$ meV (in agreement with the single-gap fit) and the putative small gap $\Delta(0) = 1.3(6)$ meV with relative weight 0.23(4). Another possibility may be some proximity contribution of the additional 4 monolayers of FeSe. Although spectroscopic data indicate that additional layers have weak interlayer coupling and do not contribute to superconductivity with the second monolayer displaying semiconducting characteristics and charge neutrality [11], superconductivity in the interfaced single-layer FeSe could induce some proximity effect at low temperature thus explaining the increase at 5 K, which is below the bulk T_c . Further measurements are needed to elucidate these questions.

To conclude, by measuring the depth and temperature dependence of the local field distribution in a heterostructure containing a buried superconducting single-layer FeSe, we detect the formation of a vortex state and quantify the superfluid density and magnetic penetration depth of single-layer FeSe. The temperature dependence can be well explained by a single BCS s -wave gap of 10.2(1.1) meV. The μ SR spectra show that the vortex state and superconductivity are homogeneously formed across the entire interface over a sample with all or the vast majority of the available charges condensing below $T_c \approx 62$ K. This shows that superconductivity in the buried interface has stable character and that inhomogeneities or imperfections of the substrate or of the overlayers do not hamper the formation of a superconducting state nor sizeably modify its properties. A very sensitive magnetic probe such as polarized muons do not see indication of static or dynamic magnetism thus supporting spectroscopic evidence that the SDW present in thin film FeSe is absent in the monolayer [11]. The simple structure of single-layer FeSe and its high T_c with s -wave BCS clean character make it an ideal system to develop a microscopic understanding of high- T_c superconductivity.

METHODS

Film growth and characterization. Single-layer FeSe thin films, each with the thickness of 0.55 nm, were grown on a $10 \times 10 \text{ mm}^2$ TiO₂ terminated and Nb-doped (0.5% wt) (001)-orientated SrTiO₃ substrate with the MBE method mentioned in ref [9]. The substrate was

pre-cleaned following the method in previous work [11] and ultrahigh vacuum (UHV) was applied during deposition to enable continuous in situ growth. The STO substrate was heated to 950°C under a Se (99.9999%) flux for 30 min in the UHV chamber after being degassed at 550 C° for three hours in ultrahigh vacuum. It was kept at 490 C° in Se and Fe (99.995%) flux for co-evaporating and co-deposition with the flux ratio of 20:1. After growth, the films were annealed at 600° in vacuum for 3h. In-situ measurements confirmed the possible 60 K superconductivity in the monolayer FeSe film (not shown here). Four more unit cells of FeSe thin films were successfully grown above the single-layer FeSe for stabilization purpose. Se films with a thickness of ~ 25 nm were then grown above the five FeSe layers for protection. Thickness of the films was monitored using a crystal oscillator and confirmed by X-ray reflectivity measurements. The μ SR measurements reported here were performed on a mosaic of 3 pieces of 10 \times 10 mm² surface area films. The samples were glued to a Ni coated Al plate and mounted onto a cold finger cryostat. Ni suppresses the SR signal from the muons not hitting the sample.

Low-energy μ SR.

To measure the local magnetic properties of the single-layer FeSe we use μ SR as a sensitive magnetic probe [30]. Fully polarized muons are implanted in the sample one at a time, where they thermalize and act as sensitive magnetic microprobe. The muon spin precesses around the local magnetic field $B(x, y, z)$ at the muon site with the Larmor frequency $\omega_\mu = \gamma_\mu B$, $\frac{\gamma_\mu}{2\pi} = 135.5$ MHz/T. The precession and relaxation of the spin ensemble leads to a temporal evolution of the polarization, which is easily detectable via the asymmetric muon decay (lifetime $\tau_\mu = 2.2$ μ s), where a positron is emitted preferentially in the direction of the muon spin at the moment of the decay. From the damped precession signal, the field distribution and the moments associated with the vortex state can be determined. To study the heterostructure, we use LE- μ SR where the energy of the muons can be tuned (~ 1 to 30 keV) to control the implantation depth in the range (~ 1 -300) nm [21, 22]. With this unique ability, the LE- μ SR technique is an ideal probe for studying the superconducting properties of the single-layer FeSe by implanting the muons on or very close to this layer. This procedure has been successfully applied to address related questions in a variety of systems and heterostructures. In particular, by varying the implantation energy of the muons, the spatial evolution of the magnetic field distribution as the flux lines emerge through the surface of a superconducting YBa₂Cu₃O_{7- δ} film has been monitored [31], superconducting proximity effects of buried cuprate layers [32], the paramagnetic Meissner effect due to spin triplet components [33] and magnetism at transition metal-molecular interfaces have been detected [34].

* Pabitra.Biswas@stfc.ac.uk; Current address: ISIS Facility, STFC Rutherford Appleton Laboratory, Harwell Science and Innovation Campus, Oxfordshire OX11 0QX, United Kingdom

† elvezio.morenzoni@psi.ch

- [1] Bednorz J. G. & Müller K. A. Possible high- T_c superconductivity in Ba-La-Cu-O system, *Z. Phys. D*, **64**, 189-193 (1986).
- [2] Schilling, A., Cantoni, M., Guo, J. D. & Ott, H. R. Superconductivity above 130 K in the Hg-Ba-Ca-Cu-O system. *Nature* **363**, 56-58 (1993).
- [3] Kamihara, Y., Watanabe, T., Hirano, M. & Hosono, H. Iron-Based Layered Superconductor La[O_{1-x}F_x]FeAs ($x = 0.05 - 0.12$) with $T_c = 26$ K. *J. Am. Chem. Soc.* **130**, 3296 (2008).
- [4] Hsu, F. C. *et al.* Superconductivity in the PbO-type structure α -FeSe. *Proc. Natl. Acad. Sci. U.S.A.* **105**, 14262-14264 (2008).
- [5] Johnston, D. C. The puzzle of high temperature superconductivity in layered iron pnictides and chalcogenides. *Adv. Phys.* **59**, 803-1061 (2010).
- [6] Paglione, J. & Greene, R. L. High-temperature superconductivity in iron-based materials. *Nat. Phys.* **6**, 645-658 (2010).
- [7] Stewart, G. R. Superconductivity in iron compounds. *Rev. Mod. Phys.* **83**, 1589-1652 (2011).
- [8] Wang, F. & Lee, D. H. The electron-pairing mechanism of iron-based superconductors. *Science* **332**, 200-204 (2011).
- [9] Wang, Q. Y. *et al.* Interface-Induced High-Temperature Superconductivity in Single Unit-Cell FeSe Films on SrTiO₃. *Chin. Phys. Lett.* **29**, 037402 (2012).
- [10] Lee, J. J. *et al.* Interfacial mode coupling as the origin of the enhancement of T_c in FeSe films on SrTiO₃. *Nature* **515**, 245 (2014).
- [11] Božović I., High-temperature superconductivity: A conventional conundrum. *Nat. Phys.*, **12**, 22 (2016).
- [12] Liu, D. F. *et al.* Electronic origin of high-temperature superconductivity in single-layer FeSe superconductor. *Nat. Commun.* **3**, 931 (2012).
- [13] He, S. L. *et al.* Phase diagram and electronic indication of high-temperature superconductivity at 65 K in single-layer FeSe films. *Nat. Mater.* **12**, 605-610 (2013).
- [14] Tan, S. Y. *et al.* Interface-induced superconductivity and strain-dependent spin density waves in FeSe/SrTiO₃ thin films. *Nat. Mater.* **12**, 634-640 (2013).
- [15] Huang, D. *et al.* Revealing the Empty-State Electronic Structure of Single-Unit-Cell FeSe/SrTiO₃. *Phys. Rev. Lett.* **115**, 017002 (2015).
- [16] Zhang, W. *et al.* Direct observation of high-temperature superconductivity in one-unit-cell FeSe films. *Chin. Phys. Lett.* **31**, 017401 (2014).
- [17] Ge, J. F. *et al.* Superconductivity above 100 K in single-layer FeSe films on doped SrTiO₃. *Nat. Mater.* **14**, 285-289 (2015).
- [18] Zhang, Z. *et al.* Onset of the Meissner effect at 65 K in FeSe thin film grown on Nb-doped SrTiO₃ substrate. *Sci. Bulletin* **60** (14), 1301-1304 (2015).
- [19] Fan, Q. *et al.* Plain s -wave superconductivity in single-layer FeSe on SrTiO₃ probed by scanning tunneling microscopy. *Nat. Phys.* **11**, 946 (2015).

- [20] Shiogai, J. *et al.* Electric-field-induced superconductivity in electrochemically etched ultrathin FeSe films on SrTiO₃ and MgO. *Nat. Phys.* **12**, 42 (2016). doi:10.1038/nphys3530
- [21] Morenzoni, E. *et al.* Low-energy μ SR at PSI: present and future. *Physica B: Condensed Matter* **289**, 653 (2000).
- [22] Prokscha, T. *et al.* The new mu E4 beam at PSI: A hybrid-type large acceptance channel for the generation of a high intensity surface-muon beam. *Nucl. Instrum. Methods Phys. Res., Sect. A* **595**, 317 (2008).
- [23] W. Eckstein, *Computer Simulations of Ion-Solid Interactions*, (Springer Verlag Berlin, Heidelberg and New York, 1991).
- [24] E. Morenzoni *et al.* Implantation studies of keV positive muons in thin metallic layers. *Nucl. Instr. and Methods* **192**, 254-266 (2002).
- [25] Sonier, J. E., Brewer, J. H. & Kiefl, R. F. μ SR studies of the vortex state in type-II superconductors. *Rev. Mod. Phys.* **72**, 769 (2000).
- [26] Clem, J. R. Two-dimensional vortices in a stack of thin superconducting films: A model for high-temperature superconducting multilayers. *Phys. Rev. B* **43**, 7837 (1991).
- [27] Brandt, E.H. Ginzburg-Landau vortex lattice in superconductor films of finite thickness. *Phys. Rev. B* **71**, 014521 (2005).
- [28] Carneiro, G. & Brandt, E. H. Vortex lines in films: Fields and interactions. *Phys. Rev. B* **61**, 6370 (2000).
- [29] Pearl, J. Current distribution in superconducting films carrying quantized fluxoids. *Appl. Phys. Lett.* **5**, 65 (1964).
- [30] Yaouanc, A. & Dalmás de Rotier, P. Muon Spin Rotation, Relaxation and Resonance. *International Series of Monographs on Physics* 147 (Oxford University Press, Oxford, 2011).
- [31] Niedermayer, Ch. *et al.* Direct observation of a flux line lattice field distribution across an YBa₂Cu₃O_{7- δ} surface by low energy muons. *Phys. Rev. Lett.* **83**, 3932 (1999).
- [32] Morenzoni, E. *et al.* The Meissner effect in a strongly underdoped cuprate above its critical temperature. *Nat. Commun.* **2**, 272 (2011).
- [33] Di Bernardo A. *et al.* Intrinsic Paramagnetic Meissner Effect Due to *s*-Wave Odd-Frequency Superconductivity, *Phys. Rev. X* **5**, 041021 (2015).
- [34] Al Ma'Mari F. *et al.* Beating the Stoner criterion using molecular interfaces, *Nature* **524**, 69 (2015).

Acknowledgments The μ SR experiments were performed at the Swiss Muon Source, Paul Scherrer Institut, Villigen, Switzerland.

Auhtors Contributions P.K.B., Z.S and E.M planned and analyzed the experiments. P.K.B., and Z.G., performed the SR measurements at PSI. E.M., T.P., A.S., Z.S., designed and developed the LE- μ SR set-up. Q.S., R.P., J.Z., L.S., D.L.F. prepared the samples at Fudan University and characterized them by ARPES. E.M. wrote the manuscript with input from P.K.B and Z.S. All authors subsequently contributed to discussion/comments of the text.

SUPPLEMENTARY INFORMATION

μ SR data analysis

Measurements were performed at zero field (ZF) and with field applied transverse to the initial muon spin polarization (TF). In a magnetic environment, well defined precession frequencies may be observed in ZF in the case of long range order or a distribution of precession frequencies with the corresponding width proportional to the field inhomogeneity. If the field distribution is broad when averaged over the sample, as in the case of disordered or short range magnetism, the muon decay asymmetry displays a fast depolarization. In the case of dynamic moments with fluctuating times within the μ SR time window relaxation is also observed. These features allow the direct observation of the onset of magnetic order even if very weak. It has been used for instance to search for time reversal symmetry breaking phenomena (TRSB) in the superconducting phase, where a very tiny spontaneous static magnetic field appears with the onset of superconductivity [1, 2]. The ZF-spectra can be described well using a static Gaussian Kubo-Toyabe relaxation function [3], where the time evolution of the asymmetry $A(t)$ which is proportional to the muon spin polarization, is given by:

$$A(t) = A(0) \left\{ \frac{1}{3} + \frac{2}{3} (1 - \sigma_{ZF}^2 t^2) \exp \left(-\frac{\sigma_{ZF}^2 t^2}{2} \right) \right\}, \quad (1)$$

where $A(0)$ is the initial asymmetry, and σ_{ZF} is the muon spin relaxation rate. Nearly equal and very small values of σ_{ZF} (0.086(5) and 0.082(5) μ s⁻¹ for 5 and 100 K, respectively), extracted from the fits for two different temperatures at 2.3 keV implantation energy, reflect the presence of random local fields arising solely from the nuclear moments within the sample.

The TF- μ SR time spectra were analyzed using a Gaussian damped spin precession signal [4]:

$$A(t) = A(0) \exp(-\sigma^2 t^2 / 2) \cos(\gamma_\mu B_{loc} t + \phi), \quad (2)$$

where $A(0)$ is the initial asymmetry, B_{loc} is the magnetic field at the muon sites, ϕ is the initial phase offset of the muon precession signal, and $\sigma(T) = (\sigma_{sc}^2(T) + \sigma_{nm}^2)^{\frac{1}{2}}$ is the Gaussian muon spin damping rate due to inhomogeneous field distribution generated in the vortex state in single-layer FeSe $\sigma_{sc} = \sqrt{\Delta B^2}$ and σ_{nm} the nuclear moment contribution. As expected in the absence of static or dynamic magnetism $\sigma_{ZF} \cong \sigma_{nm}$. Figure 7 shows the TF- μ SR time spectra collected at (a) 5 K and (b) 70 K. At 70 K, the local field probed by the muons corresponds to the applied field and only a weak damping of the signal is observable, consistent with the ZF results at 100K. By contrast, the data collected at 5 K shows a more pronounced damping. The average spin precession frequency, which is proportional to the average local field,

corresponds very closely to the applied field as expected from a demagnetizing factor close to one in this geometry.

Calculation of the field width

The magnetic field $\vec{B}(x, y, z)$ can be conveniently calculated with London theory, which is appropriate for an extreme type-II superconductor ($\xi \ll \lambda$, ξ coherence length $\sim 2\text{-}3\text{ nm}$ [5]). Here z is the coordinate perpendicular to the sample surface, parallel to the applied field ($z=0$ coordinate of the single layer), and x, y the planar coordinates. For single-layer FeSe, application of a magnetic field will lead to the formation of a regular vortex structure of hexagonal symmetry, with each vortex carrying a flux quantum Φ_0 and intervortex separation $D \equiv \sqrt{2\frac{\Phi_0}{\sqrt{3}B_0}} \cong 490\text{ nm}$ for $B_0 = 10\text{ mT}$. Indication of such a structure has been visualized by STM measurements [19]). In a bulk superconductor the local field, although varying with x and y , is always in the z direction of the applied field. In our case, near the single-layer, the field lines splay out. However, this effect on the μSR signal is small and we can consider the normal component of the field [6].

We determine $B_z(x, y, z)$ from the requirement that it fulfils London equation with source terms representing the flux lines core in a very thin superconducting film ($-d/2 < z < d/2$) and Laplace equation outside,

$$-\nabla^2 B_z(x, y, z) + \Pi(z) \frac{B_z(x, y, z)}{\lambda^2} = \Pi(z) \frac{\Phi_0}{\lambda^2} \sum_{\vec{R}} \delta(\vec{r} - \vec{R}) \quad (3)$$

where $\Pi(z)$ is the boxcar function, which is equal to 1 for $-d/2 \leq z \leq d/2$ and 0 otherwise, $\vec{r} = (x, y)$ and \vec{R} the vortex positions. The solution is obtained by Fourier transforming $B_z(x, y, z)$ in the $x - y$ plane

$$B_z(x, y, z) = \sum_{\vec{k}} b_z(\vec{k}, z) e^{-i\vec{k} \cdot \vec{r}} \quad (4)$$

where \vec{k} is the reciprocal lattice vector of the flux lattice with $k = |\vec{k}| = \sqrt{\frac{16\pi^2(m^2 - mn + n^2)}{3D^2}}$. After matching the field and its derivative at the layer boundaries, we determine the Fourier coefficients $b_z(\vec{k}, z)$ so that solutions are obtained inside and outside the single-layer FeSe. The width of the field distribution at z is then given by $\Delta B_z^2(z) = \langle B_z^2(z) \rangle - \langle B_z(z) \rangle^2 = \sum_{\vec{k} \neq 0} b_z(\vec{k}, z)^2$.

Averaging is over the x and y plane coordinates. For a comparison with the measured broadening, $\Delta B_z(z)$ has to be weighted with the normalized muon stopping distribution, which depends on implantation energy, $n(z, E)$ so that $\sigma_{\text{sc}}^2(E) = \gamma_\mu^2 \int_{-\infty}^{\infty} \Delta B_z^2(z) n(z, E) dz$.

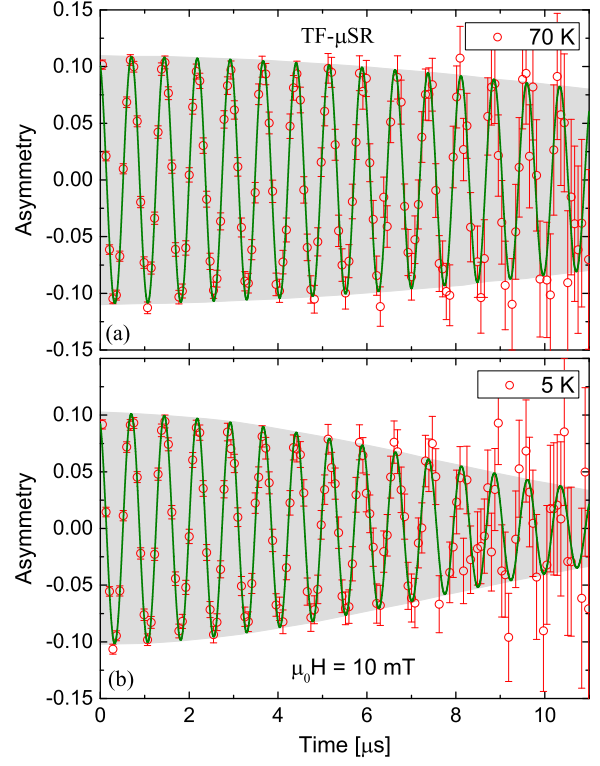


FIG. 7: **Muon spin rotation signal.** TF- μSR time spectra of single-layer FeSe collected in a transverse field of 10 mT with a muon implantation energy of 3 keV (a) 5 K and (b) 70 K. The solid lines are the fits to the data using the Eq. 2, described in the text. The shaded area evidences the different damping rate

Models for the superconducting gap symmetry

The fits of the temperature dependence of the superfluid density were made with a single s -wave model. Alternatively a two s -wave gap model was used. The functional form of the two gap model, which includes as a special case the more relevant single gap model, is [7]:

$$\frac{\lambda^{-2}(T)}{\lambda^{-2}(0)} = \omega \frac{\lambda^{-2}(T, \Delta_1(0))}{\lambda^{-2}(0, \Delta_1(0))} + (1 - \omega) \frac{\lambda^{-2}(T, \Delta_2(0))}{\lambda^{-2}(0, \Delta_2(0))}, \quad (5)$$

where $\lambda(0)$ is the value of the penetration depth at $T = 0\text{ K}$, $\Delta_i(0)$ is the value of the i -th ($i = 1$ or 2) superconducting gap at $T = 0\text{ K}$ and ω is the weighting factor of the largest gap.

Each component of Eq. 5 can be calculated within the

local London approximation ($\lambda \gg \xi$) [8, 9] as

$$\frac{\lambda^{-2}(T, \Delta_i(0))}{\lambda^{-2}(0, \Delta_i(0))} = 1 + 2 \int_{\Delta_i(0)}^{\infty} \left(\frac{\partial f}{\partial E} \right) \frac{EdE}{\sqrt{E^2 - \Delta_i(T)^2}}, \quad (6)$$

where $f = [1 + \exp(E/k_B T)]^{-1}$ is the Fermi function, and $\Delta_i(T) = \Delta_i(0)\delta(T/T_c)$. The temperature dependence of the gap is parametrized by the expression $\delta(T/T_c) = \tanh \left\{ 1.82 [1.018 (T_c/T - 1)]^{0.51} \right\}$, which well represents the temperature dependence of a BCS gap [10].

ARPES characterization

Fig. 8 shows an ARPES measurement of the FeSe monolayer before depositing the overlayers and showing the typical features of the electronic structure [11, 12].

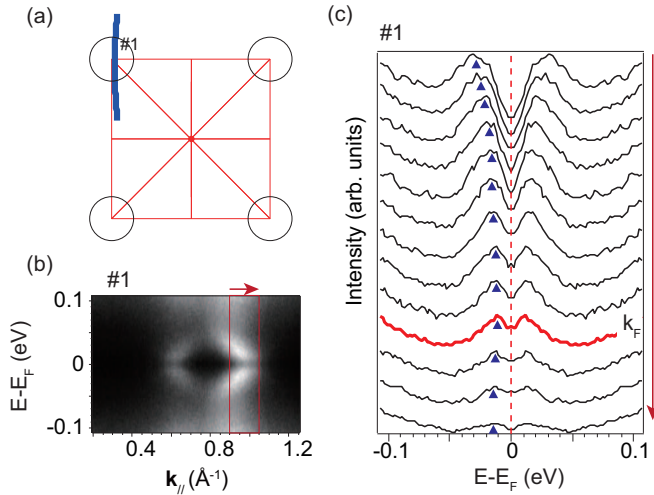


FIG. 8: **Sample characterization by ARPES measurements** (a) Sketch of the Fermi surface sheets and Brillouin zone of single-layer FeSe/STO. Cut #1 is indicated in the Brillouin zone. (b) The photoemission intensity along cut #1, which is symmetric with respect to Fermi energy. (c) Symmetrized energy distribution curves along a portion of cut #1 which is indicated by the red arrow in panel b. Data were collected at 25K.

* Pabitra.Biswas@stfc.ac.uk; Current address: ISIS Facility, STFC Rutherford Appleton Laboratory, Harwell Science and Innovation Campus, Oxfordshire OX11 0QX, United Kingdom

† elvezio.morenzoni@psi.ch

- [1] Luke, G. M. *et al.* Time-reversal symmetry breaking superconductivity in Sr_2RuO_4 . *Nature* **394**, 558 (1998).
- [2] Biswas, P. K. *et al.* Evidence for superconductivity with broken time-reversal symmetry in locally noncentrosymmetric SrPtAs . *Phys. Rev. B* **87**, 180503(R) (2013).
- [3] Kubo, R. A stochastic theory of spin relaxation. *Hyperfine Interact.* **8**, 731 (1981).
- [4] Suter A., Wojek B. M., Musrfit: A Free Platform-Independent Framework for SR Data Analysis, *Physics Procedia*. **30**, 69 (2012).
- [5] Shiogai, J. *et al.* Electric-field-induced superconductivity in electrochemically etched ultrathin FeSe films on SrTiO_3 and MgO . **12**, 42 (2016). doi:10.1038/nphys3530
- [6] Brandt, E.H. Ginzburg-Landau vortex lattice in superconductor films of finite thickness. *Phys. Rev. B* **71**, 014521 (2005).
- [7] Padamsee, H. & Neighbor, J. E. & Shiffman, C. A. Quasiparticle phenomenology for thermodynamics of strong-coupling superconductors. *J. Low Temp. Phys.* **12**, 387 (1973).
- [8] Tinkham, M. Introduction to Superconductivity. (McGraw-Hill, New York, 1975).
- [9] Prozorov, R. & Giannetta, R. W., Magnetic penetration depth in unconventional superconductors. *Supercond. Sci. Technol.* **19**, R41 (2006).
- [10] Carrington, A. & Manzano, F. Magnetic penetration depth of MgB_2 . *Physica C* **385**, 205 (2003).
- [11] Tan, S. Y. *et al.* Interface-induced superconductivity and strain-dependent spin density waves in $\text{FeSe}/\text{SrTiO}_3$ thin films. *Nat. Mater.* **12**, 634-640 (2013).
- [12] Liu, D. F. *et al.* Electronic origin of high-temperature superconductivity in single-layer FeSe superconductor. *Nat. Commun.* **3**, 931 (2012).